Immobilization Based Control of Spider-Like Robots in Tunnel Environments

Amir Shapiro
Dept. of ME, Technion
amirs@tx.technion.ac.il

Elon Rimon*
Dept. of ME, Technion
elon@robby.technion.ac.il

Shraga Shoval
Dept. of IE, Ariel College
shraga@hitech.technion.ac.il

Abstract

This paper presents an immobilization-based control method for spider-like robots that move quasistatically in tunnel environments. The control method is based on a recent immobilization theory of bodies in contact. This theory ensures that when a spider-like mechanism is bracing against the environment at an immobile posture, the naturally occurring compliance at the contacts stabilizes the mechanism as a single body. Based on this result, we present two versions of a position control law for general k-limbed robots. We show that if the controller's stiffness (i.e. proportional gain) is above a lower limit determined by the robot and environment parameters, stability of the closed-loop spider system is guaranteed. Next we present dynamic simulations of a spider robot moving in a tunnel under the influence of the immobilization-based control law. The simulations show excellent convergence properties of the control algorithm. A four-legged spider prototype has been built, and we conclude with a description of initial experiments with this prototype.

*This research was supported by grant 29-96-1 of the Israel Science Foundation.

1 Introduction

Conventional mobile robots are wheeled vehicles that require a sufficiently flat terrain in order to perform their tasks. However, many robotic tasks are more suited for legged robots that interact with the environment in order to achieve stable locomotion. For example, surveillance of collapsed structures, inspection and testing of complex pipe systems, and maintenance of hazardous structures such as nuclear reactors, all require motion in congested, unstructured, and complex environments. Furthermore, in such environments the robot cannot always rely on friction, as surfaces may be wet, oily, or icy. Our goal is to develop a general purpose multi-limbed mechanism that uses quasistatic motion to navigate in such environments. In *quasistatic motion*, inertial effects due to moving parts of the robot are kept small relative to the forces and torques of interaction between the robot and the environment. Motion is generated by reaction forces between the robot and the environment, and during this motion the robot maintains stable equilibrium with the environment.

Spider-like and snake-like mechanisms are examples of robots that can move quasistatically in congested environments. Examples of spider-like robots are the pipe-crawling robots of Neubauer [16] and Pfeiffer et al. [18, 23]. Other examples are the ladder-climbing robot of Dubowsky et al. [3, 13] and the nuclear-reactor servicing robot of Stone et al. [26]. Snake-like mechanisms are related to spider-like mechanisms, since both mechanisms brace against the environment while moving free parts toward a new position. Chrikjian and Burdick [2], Hirose and Morishima [7], and Shan and Koren [25] developed snake-like mechanisms that move by locking some of their links to the ground while allowing other links to move. Legged locomotion over a terrain is related to locomotion in congested environments. Examples of works in this area are by Boissonnat et al. [1], Hirose and Kunieda [6], Marhefka and Orin [14], McGeer [15], and Van-den-Doel and Pai [30]. However, we focus on locomotion in congested tunnel-like environments rather than legged locomotion over a terrain.

In this paper we present a control algorithm that guarantees stable locomotion of spider-like robots under the following assumptions. First, we assume that each limb of the mechanism contacts the environment only through its distal link, called the *footpad*. The footpads have no suction cups and can only push against the environment. Second, we study locomotion in *two-dimensional horizontal tunnels with piecewise linear walls*. However, real tunnel walls may be wet, oily, or icy. Hence we assume *slippery tunnel walls*, so that locomotion must proceed without using friction. This restriction excludes tunnels of a particular simple geometry (such as two parallel lines), but most unstructured congested environments do have a complex geometry with many possible footholds within reach of the robot. Furthermore, since friction always acts to *enhance* the stability of a mechanism contacting the environment, a frictionless locomotion plan can also be executed in a frictional environment. Our last assumption is that the spider moves *quasistatically*, by stably bracing itself against the tunnel walls while changing its internal configuration to allow motion of its free parts to the next position. This approach enables the robot to reliably operate even when unpredicted external forces are applied, such as drag forces from surrounding air or liquids, unexpected collisions, or uneven loads.

The control problem associated with quasistatic locomotion of spider-like robots is as follows. Consider a k-limbed spider mechanism, such that each limb has n actuated degrees of freedom. As illustrated in Figure 1, the limbs are interconnected by a central base that

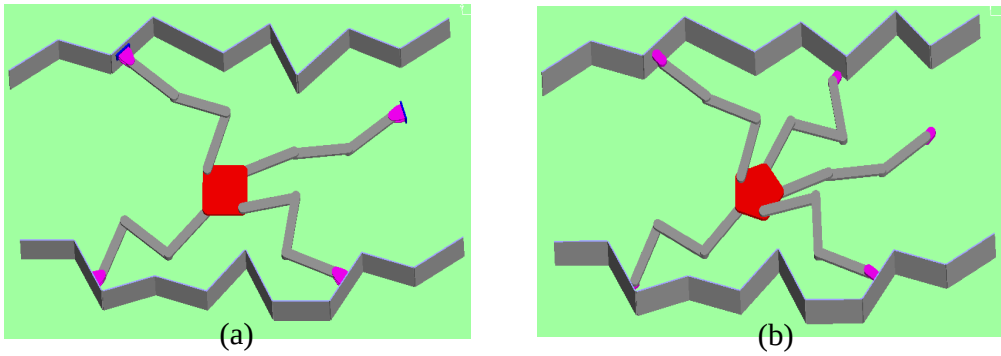

Figure 1: Conceptual designs of (a) four-legged, and (b) five-legged spider robots.

has three *unactuated* degrees of freedom. A spider robot thus has $kn+3$ degrees of freedom, of which only kn degrees of freedom are actuated. If we regard the spider's configuration space as $\mathbb{R}^{kn+3}$, the control problem is how to induce forces and torques on the spider in order to bring it to a desired configuration in $\mathbb{R}^{kn+3}$. Existing solutions to the problem make specific assumptions either on the spider's structure or the environment's geometry. Pfeiffer et al. [18, 23] assume that the spider limbs have a negligible mass relative to the central-base mass. This assumption induces a decoupling of the limbs and central-base dynamics, which allows in turn a control of the limbs' contact forces and the central-base's dynamics. It should be noted that Pfeiffer's objective is to control the limbs' contact forces with the tunnel walls, while we seek to control the spider's configuration within the tunnel. Another control approach is proposed by Dubowsky et al. [3] in the context of ladder climbing. Using Impedance Control [8], they attach virtual springs to the spider footpads and central base such that the springs' setpoints reflect the desired spider configuration. However, their approach seems to rely on the specific geometry of a ladder and lacks a formal proof of convergence.

In contrast, we present a control approach which is guaranteed to work no matter what is the mass distribution of the spider or the geometry of the environment. Our approach is based on the kinematic immobilization of the spider with respect to the tunnel walls. Using classical Form Closure theory [24, 29], four "point" footpads suffice to immobilize a mechanism by a suitable selection of the contact point positions. Figure 1(b) illustrates such an immobilizing posture for a five-legged spider. Using the recent immobilization theory of Rimon and Burdick [20, 21], a mechanism can additionally exploit surface curvature effects to immobilize itself using only three footpads. Figure 1(a) illustrates such an immobilizing posture for a four-legged spider. In both cases, the key property of immobilizing postures is that *the bracing mechanism (considered as a single rigid body) is stabilized by the compliance of the footpads and tunnel walls at the contacts.* In other words, as long as the footpads maintain an immobilizing posture with respect to the environment, the reaction forces generated by the naturally occurring compliance at the contacts stabilize the mechanism as a single rigid body. Note, however, that we are still free to guide the spider's central base and other free parts along any desired trajectory, as long as the contacting footpads maintain an immobilizing posture with respect to the environment. During this motion, the tunnel walls automatically cancel all sufficiently small inertial forces generated by the moving parts of the spider. When the moving parts reach their destination the associated inertial forces vanish, and the spider's contacting footpads settle at their precise original location.

This paper begins with a review of a configuration-space based compliant contact model which is compatible with the classical Hertz contact theory. Using this model, we demonstrate that a kinematically immobile mechanism (considered as a single rigid body) has a positive definite stiffness matrix. Then we present two versions of the immobilization-based control law. The first version is simple but requires a specification of the desired spider configuration in terms of its joint values. The second version is more intuitive and allows the use of virtual springs to specify the desired spider configuration. Next we analyze the stability of the control laws. We show that if the controller's stiffness (i.e. proportional gain) is above a lower limit determined by the spider and environment parameters, stability of the closed-loop spider system is guaranteed. Next we present dynamic simulations of a spider robot moving in a tunnel under the influence of the immobilization-based control law. The simulations take into consideration the dynamics of the spider and the compliance at the contacts, and they show excellent convergence properties of the control algorithm. A four-legged spider prototype has been built, and we conclude with a description of initial experiments with this prototype.

2 The Mechanics of Compliant Contacts

Compliant stabilization of an immobile object is the basis for the control laws presented below. In this section we review this key fact by presenting a configuration-space based model for compliant contacts. Using this model, we introduce the stiffness matrix of a compliant grasp or posture, and demonstrate that this matrix is positive definite when the grasped object or posturing mechanism is immobilized by its surrounding bodies.

2.1 Compliance Modeling

In our setup, an object $\mathcal{B}$ is held by k stationary and frictionless finger bodies $\mathcal{A}_1, \ldots, \mathcal{A}_k$ in an equilibrium grasp. Equivalently, a k-limbed mechanism is bracing itself against an environment in a static equilibrium posture. In the latter case the mechanism plays the role of $\mathcal{B}$, while the tunnel walls play the role of $\mathcal{A}_1, \ldots, \mathcal{A}_k$. We make two assumptions which are consistent with the solid mechanics literature [28]. We assume that the bodies are smooth in the vicinity of the contacts. We also assume that the bodies are *quasi-rigid*, meaning that their deformation due to compliance effects is localized to the vicinity of the contacts. The latter assumption allows us to describe the overall motion of $\mathcal{B}$ relative to the stationary bodies $\mathcal{A}_1, ..., \mathcal{A}_k$ using rigid-body kinematics. This assumption is valid for all bodies which are not made of exceptionally soft material and do not contain slender substructures.

Our compliant contact model is based on *overlap functions* introduced in Ref. [21]. These functions represent the continuous elastic deformation at a contact by a lumped parameter characterizing the inter-penetration of the undeformed bodies. Consider a single contact between $\mathcal{B}$ and $\mathcal{A}_i$. In the absence of deformation, the two bodies contact at a single point. After deformation occurs, the two bodies inter-penetrate as illustrated in Figure 2. Let $\mathcal{B}$ be at a configuration q. Then the *overlap* between $\mathcal{B}$ and $\mathcal{A}_i$, denoted $\delta_i(q)$, is *the minimum amount of translation of $\mathcal{B}$ which would separate it from $\mathcal{A}_i$*. By definition, $\delta_i(q)$ vanishes when $\mathcal{B}$ is disjoint from $\mathcal{A}_i$. When the overlap is positive and sufficiently small,

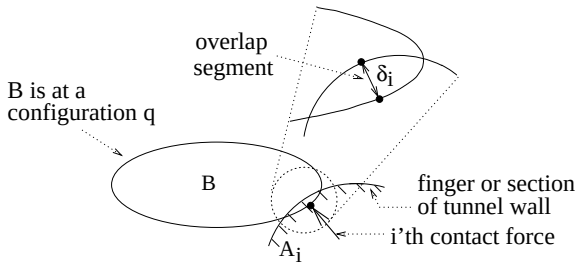

Figure 2: The overlap segment representing the inter-penetration of $\mathcal{A}_i$ and $\mathcal{B}$.

there is a unique segment, called the *overlap segment*, whose endpoints lie on the boundary of $\mathcal{B}$ and $\mathcal{A}_i$, such that the length of the segment is δ_i and its orientation gives the direction of separating translation. The overlap segment is also collinear with the normals to the boundaries of $\mathcal{B}$ and $\mathcal{A}_i$. The net contact force is assumed to act on $\mathcal{B}$'s endpoint of the overlap segment, in the direction of the overlap segment. The force's magnitude is assumed to depend on the overlap in terms of a function $f_i(\delta_i)$, which is required to be differentiable, zero when its argument is zero, and positive when its argument is positive. The simplest model assumes that f_i is a linear function of the overlap: $f_i(\delta_i) = \kappa_i \delta_i$, where the coefficient κ_i represents the combined stiffness of $\mathcal{B}$ and $\mathcal{A}_i$. While this model is linear in δ_i, it is typically *not* linear in q, since $\delta_i(q)$ is in general nonlinear in q. The Hertz model [5] which has been verified theoretically and experimentally, establishes that $f_i(\delta_i) = \kappa_i \delta_i^{3/2}$, where κ_i is a specific function of the bodies' local material and geometric properties.

Consider now an equilibrium grasp or posture, where $\mathcal{B}$ is at a configuration q_0 in contact with stationary bodies $\mathcal{A}_1, ..., \mathcal{A}_k$. Then the elastic potential energy of the system of bodies is:

$$\Pi(q) = \sum_{i=1}^{k} \int_0^{\delta_i(q)} f_i(\delta) d\delta. \tag{1}$$

It can be verified that $\delta_i(q)$ is differentiable almost everywhere, and consequently $\Pi(q)$ is twice differentiable. In the absence of a disturbing wrench (i.e. force and torque), an equilibrium at q_0 is characterized by the condition:

$$\nabla\Pi(q_0) = \sum_{i=1}^{k} f_i(\delta_i(q_0)) \nabla\delta_i(q_0) = \vec{0}, \tag{2}$$

where the gradient vector $\nabla\Pi(q_0)$ represents the derivative $D\Pi(q_0)$.

2.2 The Stiffness Matrix of a Compliant Grasp or Posture

When an object $\mathcal{B}$ is held in equilibrium grasp at a configuration q_0, the grasp's *stiffness matrix* is defined as the Hessian, $K = D^2\Pi(q_0)$, of the elastic potential energy $\Pi(q)$ at q_0. Similarly, when a mechanism $\mathcal{B}$ is bracing against the environment in static equilibrium, we may treat the mechanism as a single rigid body and then $K = D^2\Pi(q_0)$ is the posture's stiffness matrix. Since $\nabla\Pi(q_0) = 0$, the behavior of Π in the vicinity of q_0 is determined by K. If K is positive definite then Π has a local minimum at q_0 and the grasp is stable [21]. The stiffness matrix has the following well-known interpretation. When an object

$\mathcal{B}$, held in an equilibrium grasp, is subjected to a disturbing wrench $\boldsymbol{w}_{ext}$, it undergoes a displacement that can be approximated by a tangent vector $\dot{q}$. The stiffness matrix relates the displacement of $\mathcal{B}$ to the net wrench generated by the fingers' reaction forces, according to the formula $\boldsymbol{w} = -K\dot{q}$. When $\mathcal{B}$ is subjected to an external wrench $\boldsymbol{w}_{ext}$, the finger/object system settles at a nearby equilibrium where the fingers' net reaction wrench balances the external wrench. Thus, the stiffness matrix relates the displacement of $\mathcal{B}$ to the external wrench by the formula $\boldsymbol{w}_{ext} = K\dot{q}$.

To compute the stiffness matrix, we take the derivative of $\nabla\Pi(q)$ given in (2), and obtain the key formula:

$$K = \sum_{i=1}^{k} \left\{ f_i'(\delta_i(q_0))\nabla\delta_i(q_0)\nabla\delta_i(q_0)^T + f_i(\delta_i(q_0))D^2\delta_i(q_0) \right\}, \tag{3}$$

where $f_i' = df_i/d\delta_i$. General formulas for $D^2\delta_i(q_0)$ appear in Ref. [12]. We note that the first summand depends on the contact-point positions and contact-normal directions, while the second summand additionally depends on the surface curvature at the contacts. In other words, the first summand accounts for first-order geometrical effects, while the second summand accounts for second-order, or surface curvature, effects. This phenomenon has been observed at various levels of generality in Refs. [9, 17, 21].

2.3 Kinematic Immobility Implies Compliant Stability

Immobilization theory studies the mobility of a rigid object $\mathcal{B}$ grasped by rigid finger bodies $\mathcal{A}_1, ..., \mathcal{A}_k$. Roughly speaking, $\mathcal{B}$ is immobile to first-order when the bodies' first-order geometrical properties (i.e. contact point positions and contact normal directions) prevent any instantaneous motion of $\mathcal{B}$. This notion is equivalent to classical form closure [24, 29]. The object $\mathcal{B}$ is immobile to second-order when the combination of first and second-order geometrical effects (i.e. surface curvature at the contacts) prevent any instantaneous motion of $\mathcal{B}$. Immobilization theory also asserts that first and second-order geometrical effects characterize the mobility of $\mathcal{B}$ in all generic equilibrium grasps or postures [20, 21].

We now draw a connection between immobilization and compliant stability. The following theorem asserts that kinematic immobilization guarantees dynamic stability when elastic deformation at the contacts is taken into account. The theorem uses the language of grasping, but it also applies to a mechanism bracing against the environment as a single rigid body. The theorem assumes that we start with an immobilizing "unloaded" equilibrium grasp, then press the fingers against $\mathcal{B}$ along the respective contact normals. This is a reasonable assumption, since in most real grasps the contacting fingers start in an unloaded grasp, then slowly increase their contact forces until the final loaded grasp is reached.

Theorem 1 ([21]). *Let an object $\mathcal{B}$ be immobilized to first or second-order by finger bodies $\mathcal{A}_1, ..., \mathcal{A}_k$. Then there exist positive upper bounds $\delta_{1,\max}, ..., \delta_{k,\max}$ such that all equilibrium grasps obtained by pressing the fingers along the contact normals with $\delta_i \in (0, \delta_{i,\max}]$ ($i = 1, ..., k$) have a* **positive definite** *stiffness matrix.*

The theorem is demonstrated in the appendix for the case of a k-legged spider bracing against piecewise-linear tunnel walls. When the theorem is applied to grasping, the positive definiteness of the stiffness matrix implies grasp stability. That is, if a perturbing force is applied

to an immobilized object $\mathcal{B}$, the object will return to its equilibrium grasp configuration once the perturbation is removed. When the theorem is applied to a mechanism immobilized against the environment in static equilibrium, *the posture's stability is guaranteed only if the mechanism is treated as a single rigid body.* The ensuing control laws exploit this stabilization effect to induce forces and torques on the spider's unactuated central base.

3 The Immobilization Based Control Laws

In this section we present two immobilization-based control laws for k-limbed spider robots. We first describe the dynamics of spider robots, then present the control laws, and finally analyze their stability. The spider's configuration parameters are denoted as follows. The base configuration (position and orientation) is denoted $p_0 \in I\!R^3$. Each limb possesses n actuated joints, and the joints associated with the i^{th} limb are denoted $p_i \in I\!R^n$. The joint vector of the entire spider is denoted $\bar{p} \in I\!R^{kn}$, and the configuration of the entire spider (i.e. central-base configuration and joint values) is denoted $p = (p_0, \bar{p}) \in I\!R^{kn+3}$.

3.1 The Dynamics of K-Limbed Spider Robots

Our first task is to compute the inertia matrix of a k-limbed spider robot. Since the limbs are attached to a common central base, the position of the i^{th} limb is determined by the configuration parameters (p_0, p_i). Hence the total kinetic energy of the mechanism, denoted $T(p, \dot{p})$, is given by

$$T(p,\dot{p}) = \tfrac{1}{2}\dot{p}_0^T M_0(p_0)\dot{p}_0 + \sum_{i=1}^{k} \tfrac{1}{2}(\dot{p}_0, \dot{q}_i)^T M_i(p_0,p_i) \begin{pmatrix} \dot{p}_0 \\ \dot{q}_i \end{pmatrix}, \tag{4}$$

where $M_0(p_0)$ is the central-base 3×3 inertia matrix, and $M_i(p_0, p_i)$ is the i^{th} limb $(n+3)\times(n+3)$ inertia matrix. However, in general $T(p,\dot{p}) = \frac{1}{2}\dot{p}^T M(p)\dot{p}$, where $M(p)$ is the spider's *total inertia matrix*. Eq. (4) thus implies that $M(p)$ is the symmetric positive-definite matrix:

$$M(p) = \begin{bmatrix} M_0 & M_{01} & M_{02} & M_{03} & \cdot\cdot & M_{0k} \\ M_{01}^T & M_{11} & 0 & 0 & \cdot\cdot & 0 \\ M_{02}^T & 0 & M_{22} & 0 & \cdot\cdot & 0 \\ M_{03}^T & 0 & 0 & M_{33} & \cdot\cdot & 0 \\ \cdot\cdot & \cdot\cdot & \cdot\cdot & \cdot\cdot & \cdot\cdot & \cdot\cdot \\ M_{0k}^T & 0 & 0 & 0 & \cdot\cdot & M_{kk} \end{bmatrix}_{(kn+3)\times(kn+3)} \qquad \text{where } M_i = \begin{bmatrix} 0 & M_{0i} \\ M_{0i}^T & M_{ii} \end{bmatrix}.$$

The inertia matrix has a special structure which reflects the spider's kinematics. The non-zero entries in the first row and column correspond to the kinematic coupling between the central-base and each limb, and the zero entries correspond to the lack of any coupling between the spider's limbs.

Next we describe the external forces and torques that act on the spider mechanism. First, the spider's actuators apply joint torques. These torques are denoted $(0, \tau)$, where $0 \in I\!R^3$ represents the absence of central-base actuation, and $\tau \in I\!R^{kn}$ represents the nk joint torques. Second, the tunnel walls apply reaction forces on the spider's footpads. The

net wrench due to these forces is given by the negated gradient of the elastic potential energy function, $-\nabla\Pi(p)$. Finally, the spider's motion as a single rigid body incurs damping. Since we assume frictionless tunnel walls, a chief source for this damping are viscoelastic losses due to material compression at the contacts [4]. However, in our experimental apparatus the spider is supported by roller bearings against a horizontal plane, and frictional losses in these bearings is an additional source of damping. Since only the central-base configuration p_0 varies when the spider moves as a single rigid body, we write these damping effects as $(-D_0\dot{p}_0, \vec{0})$, where D_0 is a 3×3 positive-definite matrix and $\vec{0} \in I\!R^{nk}$. Summarizing all the external influences, the spider's dynamics is given by

$$M(p)\ddot{p} + B(p,\dot{p}) = \begin{pmatrix} 0 \\ \tau \end{pmatrix} - \nabla\Pi(p) - \begin{pmatrix} D_0\dot{p}_0 \\ \vec{0} \end{pmatrix}, \tag{5}$$

where $B(p,\dot{p}) = \dot{M}(p)\dot{p} - \frac{1}{2}\dot{p}^T(\frac{d}{dp}M(p))\dot{p}$ contains Coriolis and centrifugal forces.

3.2 The Control Laws

We now present two control laws for k-limbed spider robots. In order to bring all parts of a spider robot to a desired configuration, we induce forces and torque on the spider's unactuated central-base as follows. Consider for example the four-legged spider robot depicted in Figure 1(a). The spider immobilizes itself against the tunnel walls using three limbs, and it has to bring its fourth limb to a new position specified by a higher-level motion planner. During this motion, all parts of the spider are free to move, *provided that the three footpads contacting the environment remain stationary with respect to each other.* The latter condition ensures that from the perspective of the tunnel walls, the spider remains immobilized as a single rigid body throughout its motion. Since immobilization implies compliant stability, the three footpads will settle at their original position once the moving parts reach their destination. In order to realize this behavior, the motion planner specifies a sequence of immobile target configurations to the robot controller. The motion planner is not discussed in this paper. However, quasistatic motion paradigms for 4-legged and 5-legged spider robots are described in the appendix. We now proceed with the description of the control laws.

Let $p^* = (p_0^*, \bar{p}^*)$ denote the spider's desired configuration. Then the first control law is the PD rule:

$$\tau(t) = -P(\bar{p}(t) - \bar{p}^*) - D\dot{\bar{p}}(t), \tag{6}$$

where P and D are $nk\times nk$ positive-definite matrices of proportional gains and damping coefficients. The stability analysis presented below establishes bounds on the proportional gains which ensure convergence of the spider to the configuration p^*. Note that the PD rule (6) requires no cancellation of the spider's nonlinear dynamics, and as such is simple to implement. Note, too, that in the case where P and D are diagonal matrices, (6) becomes a *decentralized* control law, where each joint needs only measure its own angular state. This approach allows straightforward implementation of (6) using standard controller boards.

The PD rule (6) can also be written as $\tau(t) = -\nabla\Phi(\bar{p}) - D\dot{\bar{p}}(t)$, where $\Phi(\bar{p}) = \frac{1}{2}(\bar{p} - \bar{p}^*)^T P(\bar{p} - \bar{p}^*)$ is a quadratic potential function with a minimum at $\bar{p}^*$. The second control law generalizes the quadratic potential to any potential function $\Phi(\bar{p})$:

$$\tau(t) = -\nabla\Phi(\bar{p}(t)) - D\dot{\bar{p}}(t), \tag{7}$$

where $\Phi(\bar{p})$ is a smooth function with a local minimum at $\bar{p}^*$, and D is the same damping matrix as above. The ensuing stability analysis characterizes the properties of Φ which ensure stability. The control law (7) can be used to specify a desired controller behavior in terms of *virtual springs*. That is, we can attach three-degrees-of-freedom springs between each footpad and the central-base. These springs vary only as a function of the joint values $\bar{p}$, and they induce a potential function $\Phi(\bar{p})$ on the spider's joints. For example, in the case of a four-legged spider bracing with three limbs, we can set the contacting footpads' springs at their contact positions with respect to the central-base, and set the fourth limb's spring at its desired position with respect to the central-base. Moreover, we can attach additional *repulsive springs* between the limbs in order to prevent inter-limb collision.

3.3 Proof of Stability

Substituting the control laws in the dynamical equation (5) gives the closed-loop system:

$$M(p)\ddot{p} + B(p,\dot{p}) = -\begin{pmatrix} 0 \\ \nabla\Phi(\bar{p}) \end{pmatrix} - \nabla\Pi(p) - Q\dot{p}, \tag{8}$$

where $Q = diag(D_0, D)$ is a positive-definite damping matrix. (Note: $\nabla\Phi(\bar{p})$ is a vector in $I\!R^{nk}$ while $\nabla\Pi(p)$ is a vector in $I\!R^{nk+3}$.) Our first task is to identify the static equilibrium point of (8). Substituting $\dot{p} = 0$ in (8) gives the equilibrium condition:

$$\frac{\partial}{\partial p_0}\Pi(p_0,\bar{p}) = 0 \quad \text{and} \quad \frac{\partial}{\partial \bar{p}}\Pi(p_0,\bar{p}) = -\nabla\Phi(\bar{p}). \tag{9}$$

By construction, the motion planner specifies an immobilizing equilibrium posture for the spider, at which the footpads penetrate the tunnel walls by a small amount. This posture determines the desired spider configuration p^* which appears in the control laws. The equilibrium point of the closed-loop system is achieved by pressing the footpads against the tunnel walls at the specified contacts, until the equilibrium condition (9) is satisfied. The first part of (9) requires that the net wrench on the central-base due to the tunnel's reaction forces be zero. The second part of (9) requires that the closed-loop joint actuators balance the joint torques induced by the tunnel's reaction forces. The following lemma establishes that such a balance is achieved during penetration of the footpads along the contact normals.

Lemma 3.1. *Let p^* be a spider configuration at which m limbs ($3 \leqslant m \leqslant k$) press against the environment in an equilibrium posture. Let δ_i^* ($i = 1, ..., m$) be the footpad penetrations corresponding to p^*. Then there exist intermediate penetration values, $0 < \hat{\delta}_i < \delta_i^*$ ($i = 1, ..., m$), at which the closed-loop system (8) is at an equilibrium.*

A proof of the lemma is sketched in the appendix. Let $\hat{p}$ denote the spider's configuration at which the closed-loop system (8) is at an equilibrium. The following theorem establishes the local asymptotic stability of $\hat{p}$ under the PD control law. This stability result is a key contribution of this paper.

Theorem 2. *Let a spider mechanism brace against the environment in an immobilizing equilibrium configuration $\hat{p} \in I\!R^{nk+3}$. Then under the PD control law (6), there exist lower bounds on the proportional gains matrix P, such that for all gains above these bounds the zero-velocity state $(\hat{p}, 0)$ of the closed-loop system (8) is* **locally asymptotically stable**.

To prove the theorem, we need the following fact concerning the stability of damped mechanical systems. A Lagrangian mechanical system, $\frac{d}{dt}\frac{\partial}{\partial \dot{p}}T(p,\dot{p}) - \frac{\partial}{\partial p}T(p,\dot{p}) = \boldsymbol{w}$, is a *damped mechanical system governed by a potential energy function* when $\boldsymbol{w}(t)$ is of the form $\boldsymbol{w}(t) = -\nabla U(p) + f_d(p,\dot{p})$, where $U(p)$ is a potential energy function and $f_d(p,\dot{p})$ is a *dissipative vector field.* A vector field $f_d(p,\dot{p})$ is dissipative if it acts to reduce the total mechanical energy of the system. That is, $f_d(p,\dot{p})\cdot\dot{p} < 0$[1] along trajectories of the system. The stability result, attributed to Kelvin [11, 27], is: *the local minima of U, with zero velocity, of a damped mechanical system are local attractors of its flow.*

Proof of Theorem 2: The closed-loop spider system (8) is subjected to a composite potential energy of the form:

$$U(p) \stackrel{\triangle}{=} \Phi(\bar{p}) + \Pi(p) \quad \text{where } p = (p_0, \bar{p}).$$

In this expression, $\Phi(\bar{p}) = \frac{1}{2}(\bar{p}-\bar{p}^*)^T P(\bar{p}-\bar{p}^*)$ is the potential energy associated with the PD control law, and $\Pi(p)$ is the elastic energy associated with the deformation at the contacts. The closed-loop system (8) is also subjected to a dissipative vector field $f_d(p,\dot{p}) = -Q\dot{p}$. By Kelvin's result, local asymptotic stability is assured if we can demonstrate that the equilibrium configuration $\hat{p}$ is a local minimum of the potential energy function $U(p)$.

Since $\hat{p}$ satisfies the equilibrium condition (9), the gradient of U vanishes at $\hat{p}$. In order to show that $\hat{p}$ is a local minimum of the $U(p)$, it suffices to show that the $(nk+3)\times(nk+3)$ second-derivative matrix $D^2U(\hat{p}) = D^2\Phi(\hat{p}) + D^2\Pi(\hat{p})$ is positive definite. First consider the second derivative $D^2\Phi(\hat{p})$. We may assume that the $nk\times nk$ proportional gains matrix P is block diagonal, $P = diag(P_1, ..., P_k)$, where each P_i is an $n\times n$ matrix. In that case

$$D^2\Phi(\hat{p}) = \begin{bmatrix} 0_{3\times3} & 0 & 0 & \cdot\cdot & 0 \\ 0 & P_1 & 0 & \cdot\cdot & 0 \\ 0 & 0 & P_2 & \cdot\cdot & 0 \\ \cdot\cdot & \cdot\cdot & \cdot\cdot & \cdot\cdot & \cdot\cdot \\ 0 & 0 & 0 & \cdot\cdot & P_k \end{bmatrix}_{(kn+3)\times(kn+3)}.$$

Next we compute the matrix $D^2\Pi(\hat{p})$. Let us assume a linear compliance relationship, so that $\Pi(p) = \sum_{i=1}^{k} \frac{1}{2}k\delta_i^2(p)$, where $k > 0$ is a uniform material stiffness coefficient. The first derivative of Π is: $\nabla\Pi(p) = \sum_{i=1}^{k} k\delta_i(p)\nabla\delta_i(p)$. The second derivative of Π is:

$$D^2\Pi(p) = k\sum_{i=1}^{k} \nabla\delta_i(p)\nabla\delta_i(p)^T + \delta_i(p)D^2\delta_i(p). \tag{10}$$

Note that the expression for $D^2\Pi(p)$ is similar in form to the expression for $D^2\Pi(q)$ given in Section 2. However, $D^2\Pi(p)$ is a function of the entire spider configuration $p \in I\!R^{nk+3}$, while $D^2\Pi(q)$ is a function of a rigid-body configuration $q \in I\!R^3$. Our next task is to write expressions for the terms $\nabla\delta_i$ and $D^2\delta_i$ appearing in (10). Since δ_i depends only on the central-base configuration, p_0, and the i^{th} limb joint values, p_i, the expression for $\nabla\delta_i$ is:

[1] If $E = U + T$ is the total mechanical energy of the system, then $\dot{E} = \dot{U} + \dot{T} = \dot{U} + \boldsymbol{w}\cdot\dot{p} = f_d(p,\dot{p})\cdot\dot{p}$. Hence the condition $\frac{d}{dt}E(p(t),\dot{p}(t)) < 0$ is satisfied when $f_d(p,\dot{p})\cdot\dot{p} < 0$.

$\nabla\delta_i(p) = \left(\frac{\partial}{\partial p_0}\delta_i(p), 0, \ldots, \frac{\partial}{\partial p_i}\delta_i(p), \ldots, 0\right)$. The expression for $D^2\delta_i$ is:

$$D^2\delta_i(p) = \begin{bmatrix} \frac{\partial^2}{\partial^2 p_0}\delta_i(p) & 0 & .. & \frac{\partial}{\partial p_i}\frac{\partial}{\partial p_0}\delta_i(p) & .. & 0 \\ .. & .. & .. & .. & .. & .. \\ \frac{\partial}{\partial p_i}\frac{\partial}{\partial p_0}\delta_i(p)^T & 0 & .. & \frac{\partial^2}{\partial^2 p_i}\delta_i(p) & .. & 0 \\ .. & .. & .. & .. & .. & .. \\ 0 & 0 & 0 & 0 & 0 & 0 \end{bmatrix}_{(kn+3)\times(kn+3)} \quad \text{for } i = 1, ..., k.$$

When we substitute for $\nabla\delta_i\nabla\delta_i^T$ and $D^2\delta_i$ in (10), the resulting expression for $D^2\Pi(p)$ is:

$$D^2\Pi(\hat{p}) = \begin{bmatrix} K_{00} & K_{01} & K_{02} & .. & K_{0k} \\ K_{01}^T & K_{11} & 0 & .. & 0 \\ K_{02}^T & 0 & K_{22} & .. & 0 \\ .. & .. & .. & .. & .. \\ K_{0k}^T & 0 & 0 & .. & K_{kk} \end{bmatrix},$$

where $K_{ii} = k(\frac{\partial}{\partial p_i}\delta_i)(\frac{\partial}{\partial p_i}\delta_i)^T + k\delta_i\frac{\partial^2}{\partial^2 p_i}\delta_i$, and $K_{0i} = k(\frac{\partial}{\partial p_0}\delta_i)(\frac{\partial}{\partial p_i}\delta_i)^T + k\delta_i\frac{\partial}{\partial p_i}\frac{\partial}{\partial p_0}\delta_i$. Note that the 3×3 submatrix K_{00} represents the stiffness of the equilibrium posture when the mechanism is regarded as a single rigid body. Combining the expressions for $D^2\Phi(\hat{p})$ and $D^2\Pi(\hat{p})$, we obtain:

$$D^2U(\hat{p}) = D^2\Phi(\hat{p}) + D^2\Pi(\hat{p}) = \begin{bmatrix} K_{00} & K_{01} & K_{02} & .. & K_{0k} \\ K_{01}^T & K_{11}+P_1 & 0 & .. & 0 \\ K_{02}^T & 0 & K_{22}+P_2 & .. & 0 \\ .. & .. & .. & .. & .. \\ K_{0k}^T & 0 & 0 & .. & K_{kk}+P_k \end{bmatrix}.$$

Let us assume for simplicity that $P_i = \sigma_i I_{n\times n}$ for $i = 1, ..., k$, where σ_i is a positive parameter. In order to establish lower bounds on the σ_i's which guarantee that $D^2U(\hat{p})$ is positive definite, we write the matrix $D^2U(\hat{p})$ as the sum:

$$\begin{aligned} D^2U(\hat{p}) &= \begin{bmatrix} 0 & 0 & 0 & .. & 0 \\ 0 & K_{11}^{(P)} & 0 & .. & 0 \\ 0 & 0 & K_{22}^{(P)} & .. & 0 \\ .. & .. & .. & .. & .. \\ 0 & 0 & 0 & .. & K_{kk}^{(P)} \end{bmatrix} + \begin{bmatrix} K_{00} & K_{01} & K_{02} & .. & K_{0k} \\ K_{01}^T & K_{11}^{(N)}+\sigma_1 I & 0 & .. & 0 \\ K_{02}^T & 0 & K_{22}^{(N)}+\sigma_2 I & .. & 0 \\ .. & .. & .. & .. & .. \\ K_{0k}^T & 0 & 0 & .. & K_{kk}^{(N)}+\sigma_k I \end{bmatrix} \\ &= A + B(\sigma_1, ..., \sigma_k). \end{aligned}$$

In this decomposition, $K_{ii} = K_{ii}^{(P)} + K_{ii}^{(N)}$, where $K_{ii}^{(P)} = k(\frac{\partial}{\partial p_i}\delta_i)(\frac{\partial}{\partial p_i}\delta_i)^T$ and $K_{ii}^{(N)} = k\delta_i\frac{\partial^2}{\partial^2 p_i}\delta_i$. The matrix A consists of outer-products of the form uu^T, and is therefore positive semi-definite. Thus, $D^2U(\hat{p}) > 0$ if the matrix $B(\sigma_1, ..., \sigma_k)$ is positive definite. Let $v = (v_0, v_1, ..., v_k)$ be a vector in $\mathbb{R}^{nk+3}$, such that $v_0 \in \mathbb{R}^3$ and $v_i \in \mathbb{R}^n$ for $i = 1, ..., k$; and let $\sigma = (\sigma_1, ..., \sigma_k)$. Then the quadratic form $v^T B(\sigma)v$ can be written as:

$$v^T B(\sigma)v = v_0^T K_{00} v_0 + 2\sum_{i=1}^{k} v_0^T K_{0i} v_i + \sum_{i=1}^{k} v_i^T (K_{ii}^{(N)} + \sigma_i I)v_i.$$

Note that $v^T B(\sigma)v = v_0^T K_{00} v_0$ when $v_i = 0$ for $i = 1, ..., k$. Hence the positive definiteness of K_{00} is necessary for the positive definiteness of $B(\sigma)$. Since the mechanism is immobilized as a single rigid body, Theorem 1 implies that K_{00} is positive definite. Let $\sigma_0 > 0$ denote the minimal eigenvalue of K_{00} and, for a given matrix E, let $\|E\|$ denote the matrix norm induced by the Euclidean norm[2]. Then $v^T B(\sigma)v$ can be bounded as follows

$$v^T B(\sigma)v \geqslant \sigma_0 \|v_0\|^2 - 2\sum_{i=1}^{k} \|K_{0i}\|\|v_0\|\|v_i\| + \sum_{i=1}^{k} (\sigma_i - \|K_{ii}^{(N)}\|)\|v_i\|^2. \tag{11}$$

The first two summands in (11) can be written as follows

$$\begin{aligned} \sigma_0\|v_0\|^2 - 2\textstyle\sum_{i=1}^{k} \|K_{0i}\|\|v_0\|\|v_i\| &= \tfrac{\sigma_0}{k} \textstyle\sum_{i=1}^{k} \left(\|v_0\|^2 - 2c_i\|v_0\|\|v_i\|\right) \\ &= \tfrac{\sigma_0}{k} \textstyle\sum_{i=1}^{k} \left\{(\|v_0\| - c_i\|v_i\|)^2 - c_i^2\|v_i\|^2\right\}, \end{aligned}$$

where $c_i = k\|K_{0i}\|/\sigma_0$. Substituting this expression in the quadratic form (11) gives:

$$v^T B(\sigma)v \geqslant \sum_{i=1}^{k} \frac{\sigma_0}{k}(\|v_0\| - c_i\|v_i\|)^2 + \left(\sigma_i - \|K_{ii}^{(N)}\| - \frac{k}{\sigma_0}\|K_{0i}\|^2\right)\|v_i\|^2. \tag{12}$$

Since $\sigma_0 > 0$, the right side of (12) is positive if the coefficient of $\|v_i\|^2$ is positive. Thus we obtain the lower bound on the controller's stiffness parameters:

$$\sigma_i > \|K_{ii}^{(N)}\| + \frac{k}{\sigma_0}\|K_{0i}\|^2 \quad \text{for } i = 1, ..., k. \tag{13}$$

Any value of the σ_i's above these lower bounds guarantees that the matrix $D^2U(\hat{p})$ is positive definite, and consequently that $\hat{p}$ is a local minimum of U. □

The potential-function based control law (7) assumes a potential function $\Phi(\bar{p})$ with a local minimum at the configuration $\bar{p}^*$. The stability proof of this control law is identical to the stability proof of the PD control law, with the second-derivative matrix of Φ replacing the matrix P. This is stated in the following corollary.

Corollary 3.2. *Under the conditions of Theorem 2, let Φ be the potential function in the control law (7). Then there exist lower bounds on the eigenvalues of the second-derivative matrix $D^2\Phi$ at the equilibrium configuration $\hat{p}$, such the zero-velocity state $(\hat{p}, 0)$ of the closed-loop system (8) is locally asymptotically stable.*

Finally, the lower bounds on the controller's stiffness parameters are specified in (13) in terms of norms on submatrices of $D^2U(\hat{p})$. These submatrices depend on the partial derivatives of the footpad overlaps δ_i. To allow computation of these lower bounds, we provide in the appendix concrete formulas for the partial derivatives of δ_i.

[2]The matrix norm is defined as $\|E\| = \max\{\|Eu\|\}$ over all vectors $\|u\| \leqslant 1$.

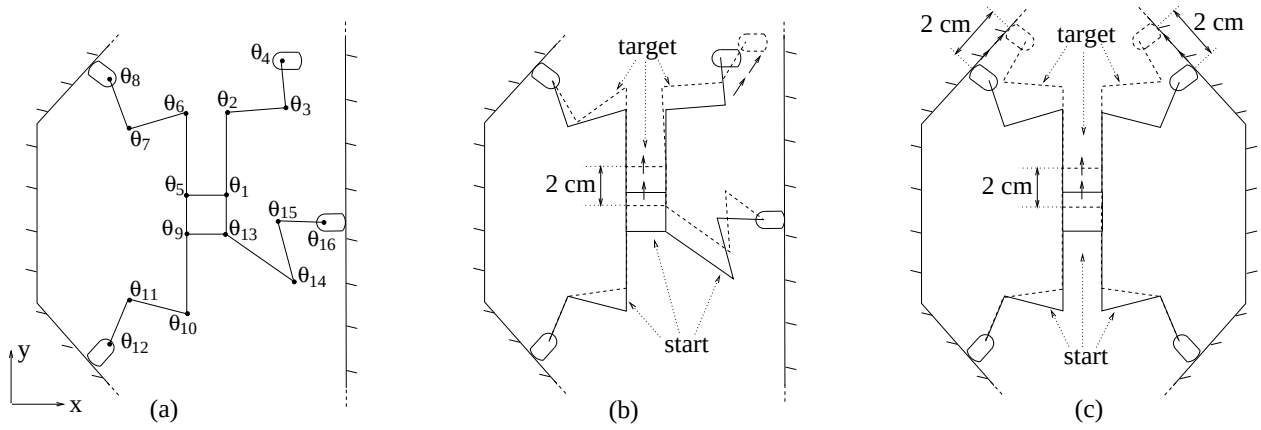

Figure 3: (a) The four-legged spider used in the simulations. The start and target postures during (b) limb lifting, and (c) limb repositioning.

4 Simulation Results

In this section we present dynamic simulations of a four-legged spider robot performing two basic motions using the PD control law. The two basic motions form the quasistatic motion paradigm described in the appendix. The first mode of motion is *limb lifting* depicted in Figure 14(a). During this motion the spider braces against the environment with three limbs while moving its fourth limb to a new foothold position. The second mode of motion is *limb repositioning* depicted in Figure 14(b). During this motion the spider slides two limbs along the tunnel walls, while the other two limbs maintain a fixed contact with the environment.

The simulations implement the closed-loop spider system using the following data. First, each limb of the spider has four revolute joints, so that the spider has a total of nineteen degrees of freedom. The central-base and links are made of Aluminum, and we neglect the mass associated with the joint motors. The central-base is a 10×10 cm square plate of thickness 12 mm. The limbs have a thickness of 12 mm and width of 36 mm, and their lengths are arranged in the following decreasing order. The link closest to the base is 24 cm long, and the next ones have lengths of 18 cm and 14 cm. The last link is a semi-circular footpad, whose length is 4 cm and whose radius-of-curvature is sufficiently large as to guarantee second-order immobilization during limb lifting. In the simulation of compliant contacts we make the following assumptions. First, we assume that the footpads are wrapped by a relatively soft material such as rubber or silicon. Using material properties of rubber [10], we linearize the Hertz compliance relationship at the pre-determined penetrations, and obtain a stiffness coefficient of $\kappa = 20$ N/mm at the contacts. This stiffness coefficient is consistent with the one used by Pfeiffer et al. [18]. Using this stiffness coefficient, we assume linear compliance where the i^{th} reaction force is linearly proportional to the penetration δ_i. Finally, we compute the wrench generated by the tunnel's reaction forces using the formula $\nabla\Pi(p) = \sum_{i=1}^{k} \kappa\delta_i(p)\nabla\delta_i(p)$, where the expression for $\nabla\delta_i(p)$ is given in the appendix.

Control of limb-lifting motion. In this example the spider is bracing with three limbs against the environment at the immobilizing equilibrium posture shown in Figure 3(b). The spider's task is to retain its contacting footpads stationary, while moving its central-base

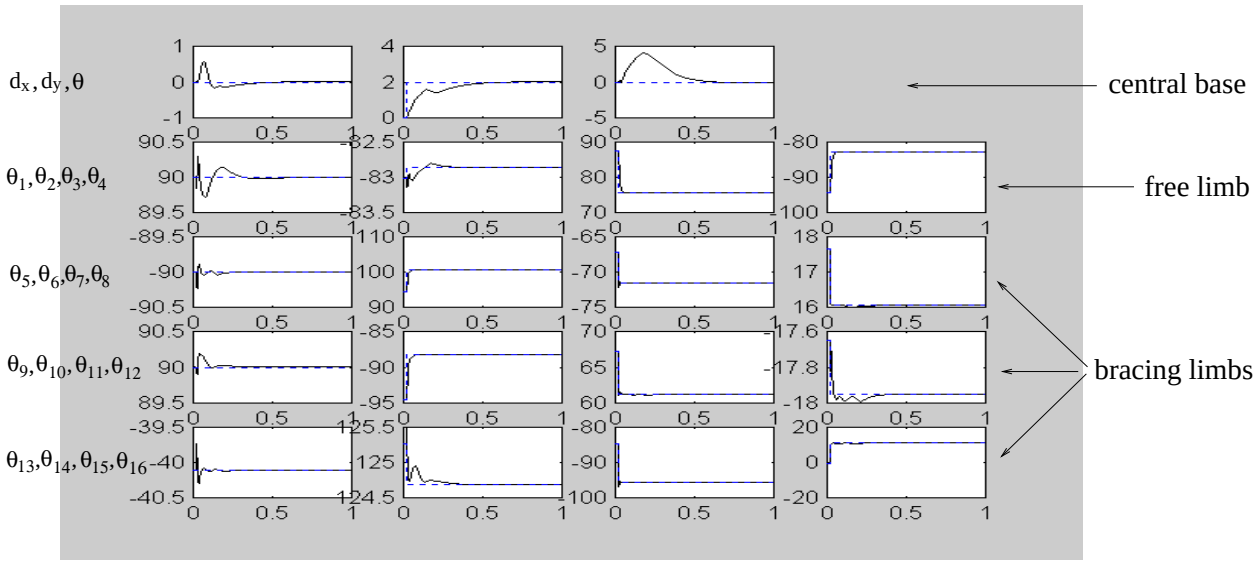

Figure 4: The spider's configuration parameters during limb lifting. Central-base position is given in cm, angles in degrees.

two centimeters ahead and bringing its free limb to the desired position depicted in the figure. In the running of this task, we used the PD law (6) with a 16×16 proportional gains matrix $P = \mathsf{diag}(18, 15, 13, 12, 18, 15, 13, 12, 18, 15, 13, 12, 18, 15, 13, 12) * 10^2$ Nm/rad. We also used a 19×19 damping matrix $Q = \mathsf{diag}(1.5, 1.5, 70, 850, 825, 85, 85, 850, 825, 85, 85, 850, 825, 85, 85, 850, 825, 85, 85) * 10^{-2}$, where the first two entries are given in N·sec/m, and the remaining entries in Nm·sec/rad.

The results of running the closed-loop spider system appear in Figure 4 and Figure 5. In these figures, the spider's joints are denoted $\theta_1, .., \theta_{16}$ as depicted in Figure 3(a). Figure 4 shows the time history of the central-base position and orientation and the sixteen joint angles. Time is measured in seconds, position in centimeters, and angles in degrees. The graphs indicate a convergence of all configuration parameters to their desired values with zero velocity in less than 0.6 seconds. Note that the central-base orientation is the slowest parameter to converge. This behavior can be expected, since the convergence of the central-base is achieved through immobilization of the spider as a single rigid body by the tunnel walls. In this immobilization, first-order geometrical effects immobilize the central-base position, while second-order or curvature effects immobilize the central-base orientation. Using an energy-based argument to compare forces and torques, it has been shown in Ref. [12] that second-order immobilizing effects are typically *weaker* than first-order effects, except in the limit where the contacting bodies have a closely matched curvature.

Figure 5 shows the time history of the actuator torques at the sixteen joints. It can be seen that the motors' maximum torque rarely exceeds 20 Nm, which is a reasonable torque for small geared motors. Finally, we have tested the sensitivity of the PD control law to actuator saturation. Using the same task specification as above, we truncated the actuator torques at various values below ±20 Nm. As shown in Figure 6, a significant degradation in the spider's convergence occurs only at truncation values of ±2 Nm. Intuitively, this

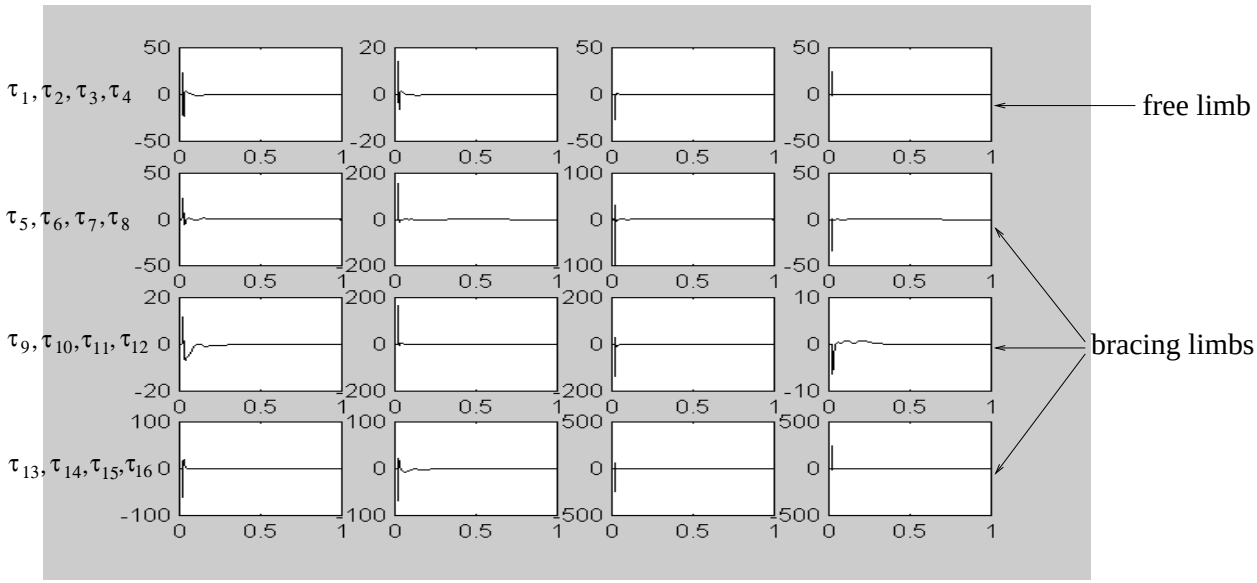

Figure 5: The spider's sixteen joint actuator torques during limb lifting. All torques are given in Nm.

insensitivity to actuator saturation is due to the relatively short high-torque durations during convergence of the closed-loop spider system.

Control of limb-repositioning motion. In this example the spider is bracing against the tunnel walls using its four limbs. As shown in Figure 3(c), the spider's task is to maintain two footpads stationary, while sliding its other two footpads along the tunnel walls to positions located two centimeters ahead. In the running of this task, we have used the PD law (6) with a proportional gains matrix $P = \mathsf{diag}(20, 5, 3, 2, 20, 5, 3, 2, 20, 5, 3, 2, 20, 5, 3, 2) * 10^2$ Nm/rad, and a damping matrix $Q = \mathsf{diag}(1, 1, 1, 500, 100, 20, 5, 500, 100, 20, 5, 500, 100, 20, 5, 500, 100, 20, 5) * 10^{-2}$, where the first two entries are given in N·sec/m, and the remaining entries in Nm·sec/rad.

The results of running the closed-loop spider system appear in Figure 7. Note that in this simulation the convergence time is about 0.2 seconds, which is shorter than the convergence time during three-legged immobilization. This shorter convergence time can be expected, since during four-legged immobilization both position and orientation of the central-base are stabilized by first-order effects. In contrast, during three-legged immobilization the central-base orientation is stabilized by second-order effects. Although the simulations show excellent convergence of the sliding footpads to their desired positions, the footpads do not slide along the walls but rather oscillate about the wall-segments while converging to their target points. Thus the simple PD rule (6), while guaranteeing convergence, gives a behavior that only approximates true sliding.

The final simulation, not shown here, executes both modes of motion assuming that the footpads and tunnel walls are made of Aluminum. A linearization of the Hertz contact model yields a stiffness coefficient of $\kappa = 4.5 \times 10^3$ N/mm. In this case we observed a convergence time of 0.05 seconds, which is an order-of-magnitude shorter than the convergence time for

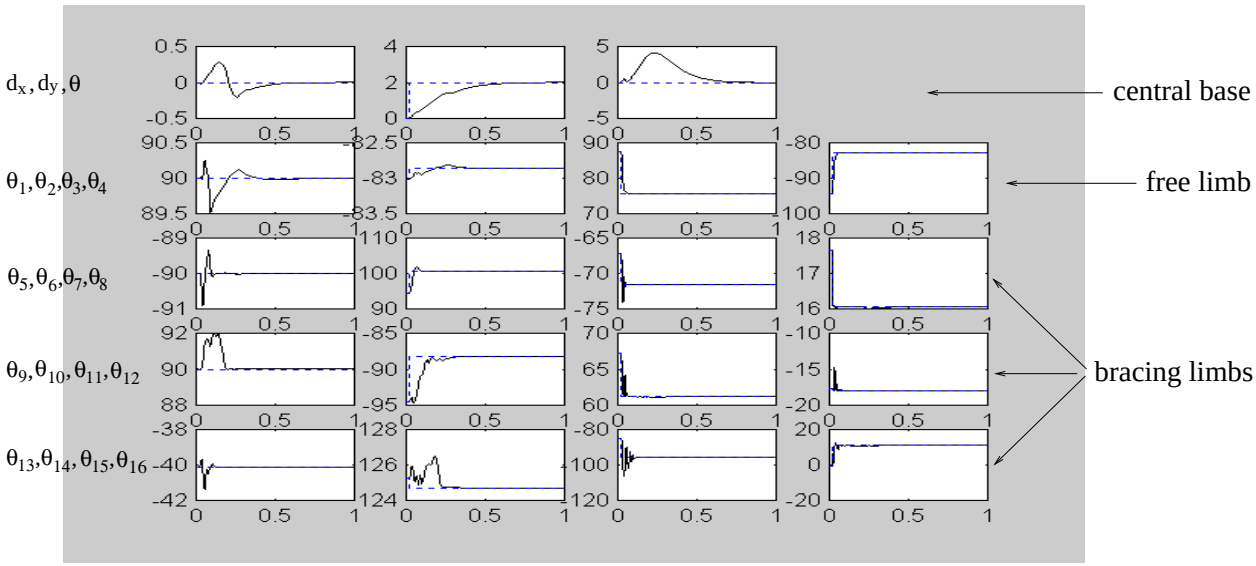

Figure 6: The spider's configuration parameters during limb lifting, with motor saturation at ± 2 Nm.

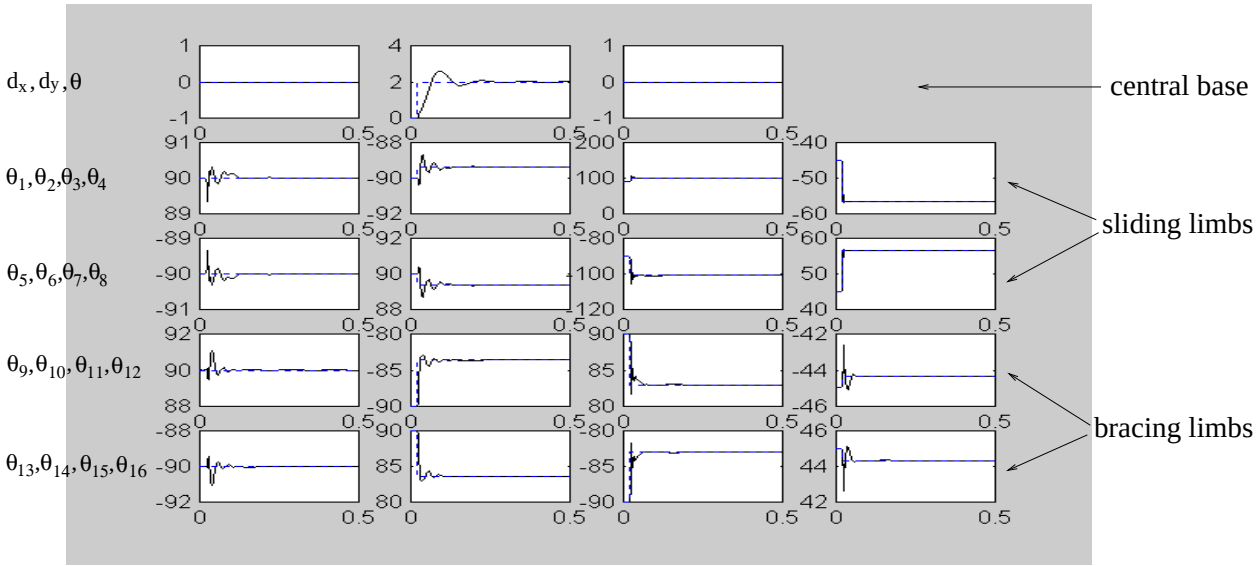

Figure 7: The spider's configuration parameters during limb repositioning. Central-base position is given in cm, angles in degrees.

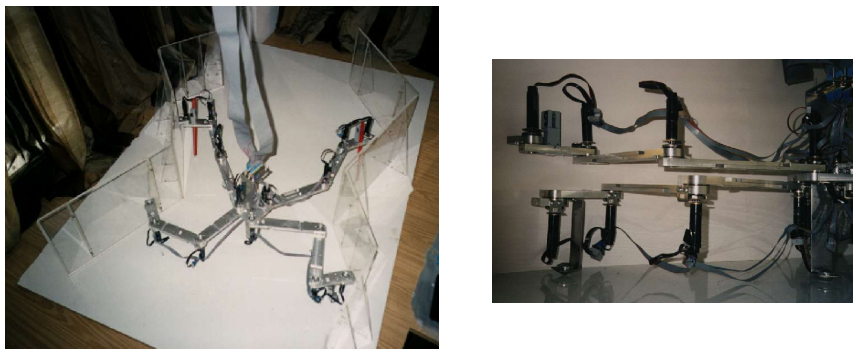

Figure 8: Snapshots showing top and side views of the spider bracing against tunnel walls.

footpads made of rubber. However, we also observed oscillations with higher frequency during convergence. This can be explained by analogy with a linear mass-spring system, whose natural frequency is monotonically increasing with the spring's stiffness. In our case the use of Aluminum rather than rubber increases the footpads' stiffness, with a corresponding increase in the frequency of oscillations during convergence. Finally, we note that a higher overall stiffness can also be achieved by pressing the footpads harder against the tunnel walls, since according to the Hertz contact model the stiffness matrix is proportional to the penetrations at the contacts.

5 Experimental Results

We describe in this section locomotion experiments conducted with a four-legged spider robot built in our laboratory. The spider prototype, shown in Figure 8, has four actuated joints in each limb, or a total of sixteen actuated joints. The mechanism is actuated by small Maxon DC servo-motors each having a magnetic encoder. The spider robot moves inside a piecewise-linear tunnel constructed on a horizontal plane, and the central-base position and orientation is measured by a CCD camera mounted above the experiment.

The first experiment executes a limb-lifting motion under the PD law (6). During this motion the spider braces against the environment in a 3-legged equilibrium posture while its fourth limb moves to a new foothold position. The entire motion was divided into fifteen intermediate targets that move the free limb along a pre-planned path while translating the central-base 25 cm forward with fixed orientation. Figure 9(a) shows the spider's start and target configurations, as well as measurements of the central-base location during this motion. The total motion took 63 seconds to complete, and measurements of the spider's configuration parameters appear in Figure 10. Note, in particular, that the central-base orientation hardly changes during this motion.

The second experiment executes a limb-repositioning motion using the PD law (6). During this motion the spider slides two footpads along the tunnel walls while the other two footpads remain stationary with respect to the environment. In this experiment the entire motion was divided into five intermediate targets that slide two footpads 10 cm along the tunnel walls. Figure 9(b) shows the spider's start and target configurations, as well as measurements of the central-base location during this motion. The total motion took

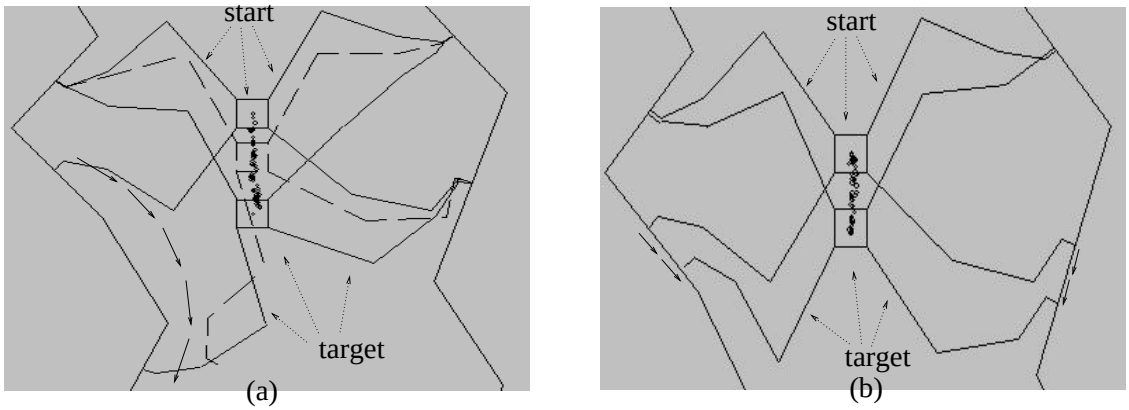

Figure 9: Measurements of the spider's central-base position during (a) limb lifting, and (b) limb repositioning experiments.

10 seconds to complete, and measurements of the spider's configuration during this motion appear in Figure 10. Both experiments corroborate the stable behavior of the immobilization-based PD control law as predicted in the analysis and simulations.

Next we consider the robustness of the closed-loop spider system with respect to small footpad placement errors. Such errors are particularly important in 3-legged equilibrium postures, since arbitrarily small placement errors yield force-lines that do not intersect at a common point as required for equilibrium. In order to compensate for such errors, we exploit friction which is present even in a small amount at the contacts. Friction effects induce a neighborhood of footpad placements about the nominal frictionless placement that hold the mechanism in a stable 3-legged equilibrium[3]. To see this fact, consider the frictionless 3-legged equilibrium posture depicted in Figure 12. The force-lines intersect at p, the i^{th} contact force magnitude is F_i, and the distance between the i^{th} contact point and p is ρ_i. Let a footpad with index i_0 be placed at a distance δ from its nominal position along the tunnel wall. Then the torque about p induced by the placement error δ is: $\eta = \delta F_{i_0}$. If we assume frictional contacts, these contacts generate tangential forces that compensate for the torque η. Let f_i denote the magnitude of the i^{th} frictional force. Then the frictional torque about p is $\rho_i f_i$, and for equilibrium of torques about p we must have $\eta = \sum_{i=1}^{3} \rho_i f_i$. Letting μ be the coefficient of friction, $f_i \leqslant \mu F_i$ according to the Coulomb friction law. Substituting the inequality $f_i \leqslant \mu F_i$ in the equilibrium condition gives: $\delta \leqslant (\mu \sum_{i=1}^{3} \rho_i F_i)/F_{i_0}$. Any footpad placement error δ satisfying this inequality would be compensated by friction effects and still generate a stable equilibrium posture. Since the contact forces have approximately the same magnitude, we obtain the approximate equilibrium condition $\delta \leqslant \mu \sum_{i=1}^{3} \rho_i$. Interpreting this inequality as a condition on the coefficient of friction μ, we obtain $\mu \geqslant \delta / \sum_{i=1}^{3} \rho_i$. In our experiments δ is in the range of a few millimeters while $\sum_{i=1}^{3} \rho_i$ is in the range of tens of centimeters. Substituting $\delta = 10$ mm and $\sum_{i=1}^{3} \rho_i = 100$ cm gives that a small coefficient of friction $\mu = 0.01$ already suffices to compensate for reasonable footpad placement errors.

We now describe experiments that verify the friction-based error compensation approach. In our experiments the footpads are made of Aluminum while the tunnel walls are

[3] Frictional equilibrium postures are force-closure stable, which is a weaker form of stability than frictionless immobilization.

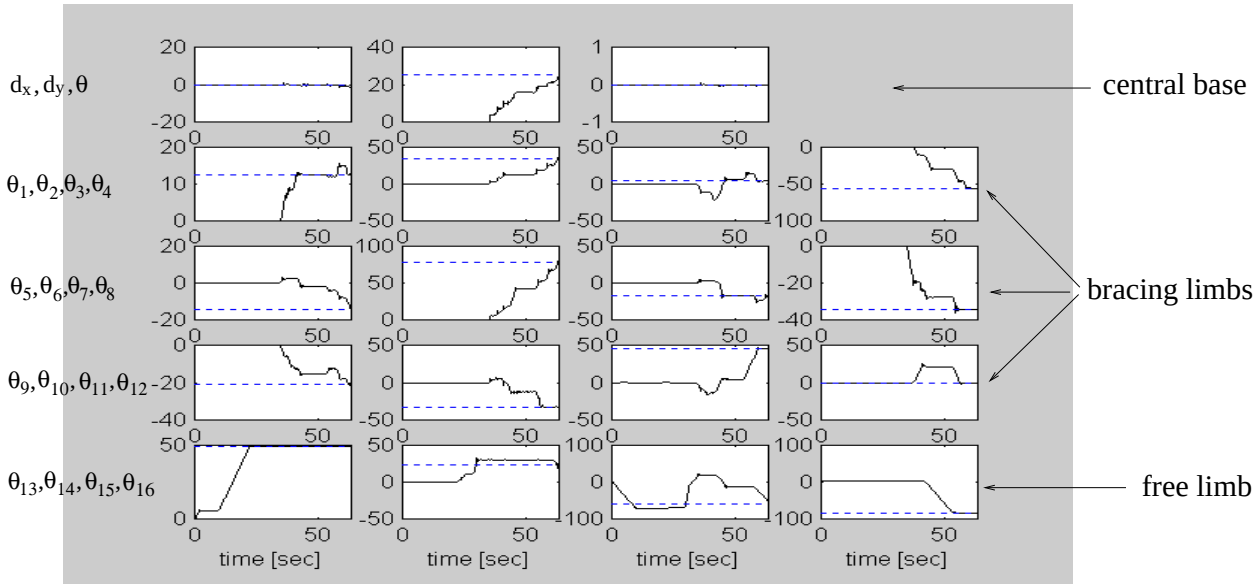

Figure 10: Measurements of the spider's configuration parameters during a limb-lifting experiment. The target configuration is indicated by horizontal lines.

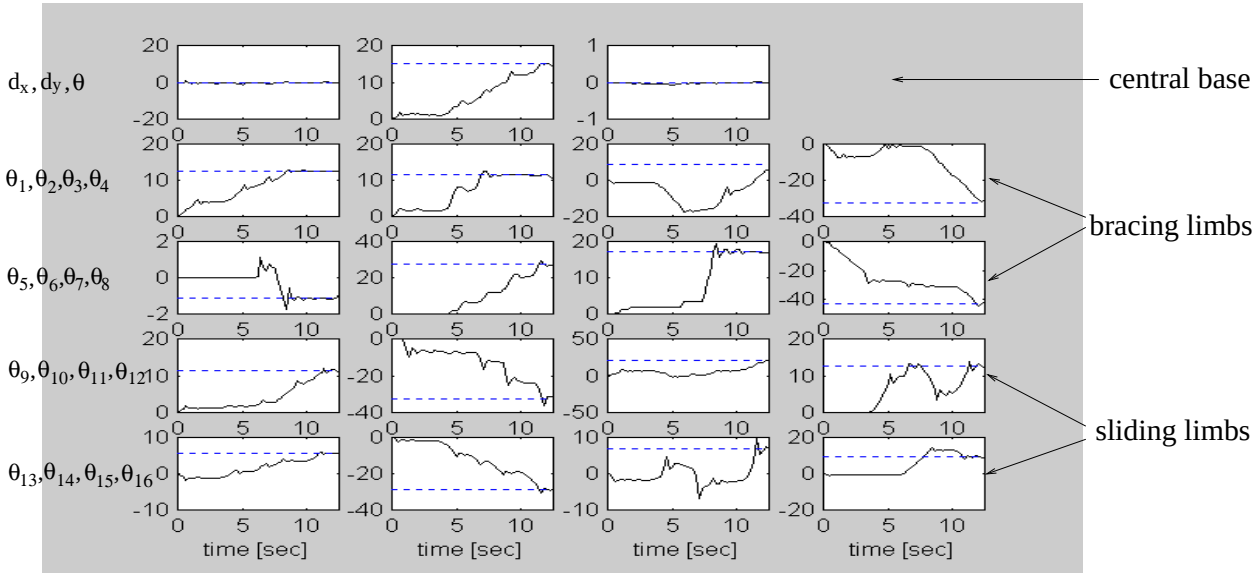

Figure 11: Measurements of the spider's configuration parameters during a limb-repositioning experiment. The target configuration is indicated by horizontal lines.

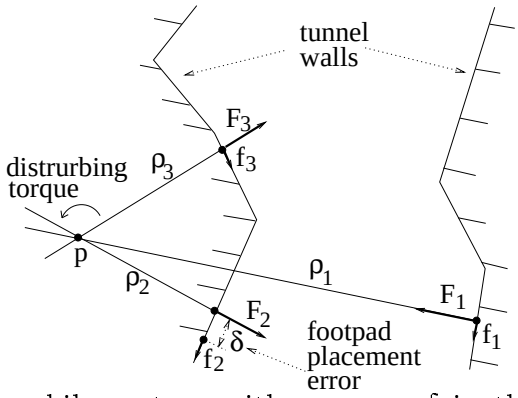

Figure 12: A 3-legged immobile posture with an error δ in the placement of the second footpad (only the contact points are shown).

made of thick Perspex plates. The coefficient of friction between the footpads and tunnel walls was originally $\mu = 0.3$. This coefficient was reduced to $\mu = 0.1$ by lubricating the tunnel walls with Teflon spray. In the first experiment we tested the 3-legged equilibrium posture depicted in Figure 12, using distances of $\rho_1 = 132.6$ cm, $\rho_2 = 50.3$ cm, and $\rho_3 = 53.4$ cm. We varied the placement error of the second footpad by increments of 5 mm, and obtained stable equilibrium postures up to a distance of $\delta = 55$ mm from the nominal footpad position. (Larger placement errors were hard to verify due to kinematic reachability constraints of the mechanism.) Next we tested the central-base position error at the end of a straight-line motion. Using the PD law (6), the spider braced with three limbs against the tunnel walls while its central-base was commanded to move 70 mm along the tunnel's central axis. The central-base position error at the end of the motion remained within a few millimeters for footpad placement errors of up to $\delta = 10$ mm. Beyond this value, inertial forces generated during the spider's motion dominated the small frictional forces at the contacts. These inertial forces caused local slips at the contacts, with a resulting large error in the central-base final position. In contrast with 3-legged immobilization, 4-legged equilibrium postures are *inherently robust* with respect to footpad placement errors. Once a nominal 4-legged equilibrium posture is established, all nearby footpad placements are automatically equilibrium postures, even in a frictionless environment. Moreover, almost all 4-legged equilibrium postures are immobile. Hence one expects a significantly better motion accuracy during 4-legged immobilization. To test this expectation, we commanded the spider's central-base to move 55 mm along a straight-line motion under the influence of the PD law (6). The central-base final position error was within few millimeters for footpad placement errors of up to $\delta = 70$ mm. Additional experimental results appear in Ref. [22].

To summarize, the experiments in both types of immobilization show robustness of the closed-loop spider system with respect to footpad placement errors in the range of a few millimeters for 3-legged immobilization and a few centimeters for 4-legged immobilization. However, robustness during 3-legged immobilization is achieved by exploiting friction effects at the contacts, an approach that deviates from our formal assumption of frictionless footpads. Indeed, we discuss in the concluding section our current research which is concerned with the inclusion of friction effects into the locomotion.

6 Concluding Discussion

We described an immobilization based control method for spider-like robots that move quasistatically in frictionless tunnel environments. In order to induce forces and torques on the spider's unactuated central-base, we used an immobilization theory that determines the conditions under which a mechanism is immobile as a single rigid body against the environment. When compliance at the contacts is taken into account, immobility yields passive stabilization of the mechanism as a single rigid body. Using this result, we presented two control laws for general k-limbed spider robots. The first law is a simple PD rule. The second law generalizes the PD rule to potential functions that can be specified via virtual springs. We showed that both laws are locally stable, provided that the controller's proportional gains are higher than a lower bound specified in terms of the spider and environment parameters. Dynamic simulations of the PD law show excellent convergence of the closed-loop spider system during three and four-legged immobilization. However, convergence of the central-base orientation is slower during three-legged immobilization, since in this case stabilization is achieved with second-order rather than first-order effects. This result highlights the trade-off incurred in the design of multi-limbed robots. A spider robot with a small number of limbs has a simpler structure and better maneuverability in congested environments. On the other hand, a smaller number of contacts requires more precise control of the robot's interaction with the environment, with contact forces that typically yield slower convergence.

The immobilization based control method is general, simple to implement, and has excellent convergence properties. We now mention several caveats in this control method which are currently under investigation. First, we provide a lower bound for the controller's stiffness parameters that guarantee stability, but do not specify how to select optimal values for these parameters. Second, the control laws guarantee convergence of the closed-loop spider system to a desired configuration, but lack the ability to track a desired trajectory. Last, immobilization-based control of spider robots moving in *three-dimensional* tunnel environments requires a more thorough consideration of the mechanics of damping. In a frictionless environment the only source of external damping is viscoelastic loss at the contacts [4]. In our simulations and experiments we relied on more significant damping introduced by friction at the roller bearings supporting the spider mechanism against a horizontal plane. In order to ensure adequate damping of the mechanism in three-dimensions, we must identify other sources of damping, such as the one incurred by micro-slip at the contacts.

Future extensions of this work will focus on the inclusion of *friction and gravity* into the locomotion. The inclusion of friction will allow the spider to move in tunnels of a particular simple geometry such as two parallel lines, as is often the case in man-made environments. However, the inclusion of friction raises several technical challenges. The first challenge is to efficiently estimate the amount of friction in a particular foothold area. A second challenge is how to guarantee adequate disturbance rejection with frictional contacts, given the bounded-torque capability of the spider's actuators. A third challenge is the need to develop a method for controlling the spider's contact forces with the environment, as to prevent slip at the contacts [18]. Note that in our immobilization-based approach the controller has the simpler task of merely maintaining the footpads at a desired position. Finally, in order to include gravity in the experiments, we plan to tilt the horizontal tunnel-plane by 45°, so that gravity would act in the plane of the two-dimensional tunnel. As long as the spider braces itself

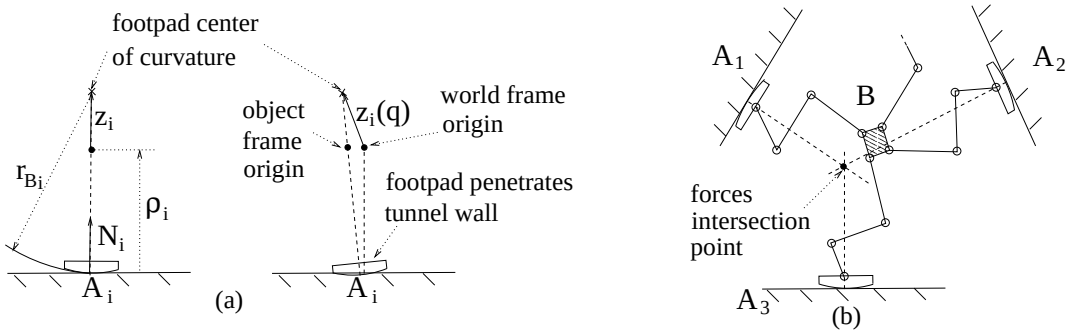

Figure 13: A 3-legged spider bracing as a single rigid body against tunnel walls.

against the tunnel walls during locomotion, the inclusion of gravity should require only minor modifications to the spider's horizontal control algorithms.

A The Stiffness Matrix of an Immobile Posture

In this appendix we verify Theorem 1 by computing the stiffness matrix of a spider mechanism bracing against piecewise-linear tunnel walls. We treat the mechanism as a single rigid object $\mathcal{B}$ whose configuration (position and orientation) is parametrized by $q = (d, \theta) \in I\!R^3$. The world and object frames are such that $\mathcal{B}$'s equilibrium configuration, q_0, is parametrized by $d = 0$ and $R(\theta) = I$. We assume a linear compliance relationship, $f_i(\delta_i) = \kappa\delta_i$, with a uniform material stiffness $k > 0$. Consider for simplicity a spider mechanism with semi-circular footpads. As shown in Figure 13(a), z_i denotes the center-of-curvature of the i^{th} footpad expressed in $\mathcal{B}$'s frame, and $z_i(q)$ denotes the same point expressed in the world frame. The two representations of the footpad's center-of-curvature are related by a rigid-body transformation, $z_i(q) = R(\theta)z_i + d$, where $q = (d, \theta)$. The i^{th} tunnel wall is a linear segment with an outward unit normal N_i. Hence the overlap δ_i is simply the projection of the vector $z_i(q) - z_i(q_0)$ along the negated normal $-N_i$. Thus $\delta_i(q) = \delta_i(q_0) + (z_i(q) - z_i(q_0)) \cdot (-N_i) = \delta_i(q_0) + z_i(q_0) \cdot N_i - (R(\theta)z_i + d) \cdot N_i$. The first and second derivatives of δ_i are:

$$\nabla\delta_i(q) = -\begin{pmatrix} N_i \\ N_i \times Rz_i \end{pmatrix} \quad \text{and} \quad D^2\delta_i(q) = \begin{bmatrix} 0_{2\times2} & 0 \\ 0 & Rz_i \cdot N_i \end{bmatrix}, \tag{14}$$

where $u \times v$ is the scalar-valued operation analogous to vector cross product, given by $u \times v = \det[u\, v]$. Substituting the derivatives of δ_i together with $f_i(\delta_i) = k\delta_i$ in the stiffness matrix formula (3) gives:

$$K = \sum_{i=1}^{k} \left\{ \begin{pmatrix} N_i \\ N_i \times z_i \end{pmatrix} \begin{pmatrix} N_i \\ N_i \times z_i \end{pmatrix}^T + \delta_i(q_0) \begin{bmatrix} 0 & 0 \\ 0 & z_i \cdot N_i \end{bmatrix} \right\} = K_1 + K_2, \tag{15}$$

where we also substituted $R = I$ and factored out the positive coefficient κ.

We wish to verify that first and second-order immobility of $\mathcal{B}$ implies positive definiteness of the stiffness matrix K (a condition written as $K > 0$). First consider the case where $\mathcal{B}$ is immobile to first-order. First-order immobilization of $\mathcal{B}$ means that the first-order approximation to the finger c-obstacles[4] isolate the equilibrium configuration q_0. Let $\mathrm{n}_i(q_0)$

[4]The *c-obstacle* due to $\mathcal{A}_i$ is the set of all configurations where $\mathcal{B}$ intersects the stationary body $\mathcal{A}_i$.

denote the outward unit normal to the i^{th} c-obstacle at q_0. Then first-order immobilization by k contacts is equivalent to the condition that the 3×3 matrix $\sum_{i=1}^{k} \mathrm{n}_i(q_0)\mathrm{n}_i(q_0)^T$ is positive definite. However, in general the wrench generated by the i^{th} contact force is a positive multiple of the unit normal $\mathrm{n}_i(q_0)$. Since the i^{th} wrench is collinear with $\nabla\delta_i(q_0)$, we can write $\nabla\delta_i(q_0) = s_i\mathrm{n}_i(q_0)$ where s_i is a scaling factor. Using this relation, the matrix K_1 can be written as $K_1 = \sum_{i=1}^{k} s_i^2\mathrm{n}_i(q_0)\mathrm{n}_i(q_0)^T$. Since $\sum_{i=1}^{k} \mathrm{n}_i(q_0)\mathrm{n}_i(q_0)^T > 0$, the matrix K_1 is also positive definite, and consequently $K = K_1 + K_2 > 0$ for all sufficiently small overlaps $\delta_i(q_0)$. Finally, the equilibrium condition (2) implies that the unit normals $\mathrm{n}_1(q_0), \ldots, \mathrm{n}_k(q_0)$ are linearly dependant. Hence the number of contacts must be at least *four* for first-order immobilization.

Consider now the case where $\mathcal{B}$ is immobile to second-order. In this case the number of contacts is either *two or three*, and the matrix K_1 is only positive semi-definite. The null space of K_1 consists of instantaneous motions along which the object can possibly break-away from the finger bodies. (All other instantaneous motions of $\mathcal{B}$ are prevented by first-order effects.) Let us consider the case of a 3-contact equilibrium posture. In this posture the three force-lines necessarily intersect at a common point (Figure 2(b)). The subspace of possible break-away motions consists of instantaneous rotations of $\mathcal{B}$ about the force-lines' intersection point. Second-order immobilization means that motions of $\mathcal{B}$ along this subspace are blocked by the finger c-obstacles when the second-order approximation to the c-obstacles is included in the analysis. This second-order approximation depends on the curvature of the contacting bodies as follows. Let us select the world and object frames at the intersection point of the force lines. Under this frame selection each vector z_i is collinear with N_i. Hence we write $z_i \cdot N_i = r_{B_i} - \rho_i$, where r_{B_i} is the i^{th} footpad radius, and ρ_i is the signed distance of the i^{th} contact from the forces' intersection point (Figure 2(a)). In the three-contact equilibrium posture, a sufficient condition for second-order immobilization is that the weighted sum $\sum_{i=1}^{k} \delta_i(q_0)(r_{B_i} - \rho_i)$ be strictly positive. Substituting for $z_i \cdot N_i$ in (15) gives:

$$K = \begin{bmatrix} \sum_{i=1}^{k} N_i N_i^T & 0 \\ 0 & 0 \end{bmatrix} + \begin{bmatrix} 0 & 0 \\ 0 & \sum_{i=1}^{k} \delta_i(q_0)(r_{B_i}-\rho_i) \end{bmatrix} = \sum_{i=1}^{k} \begin{bmatrix} N_i N_i^T & 0 \\ 0 & \delta_i(q_0)(r_{B_i}-\rho_i) \end{bmatrix} \qquad (16)$$

Second-order immobilization implies that the rotational stiffness entry in (16), $\sum_{i=1}^{k} \delta_i(q_0)(r_{B_i}-\rho_i)$, is strictly positive. (A sufficient condition would be $r_{B_i} > \rho_i$ for $i = 1, ..., k$.) Since the 2×2 translational stiffness entry in (16) is positive definite, the entire matrix K is positive definite as guaranteed by Theorem 1. Finally, we note that similar stiffness-matrix computations appear in Refs. [12, 19] in the context of grasping.

B The Spider Robot Motion

In this appendix we briefly describe quasistatic motion paradigms for two types of spider robots. The first type is the five-legged spider robot depicted in Figure 1(a). At every motion instant, this robot immobilizes itself with four limbs while lifting its fifth limb to a new position. It can be verified that any non-degenerate 4-contact equilibrium posture is automatically immobilizing, no matter what is the particular geometry of the contacts. This

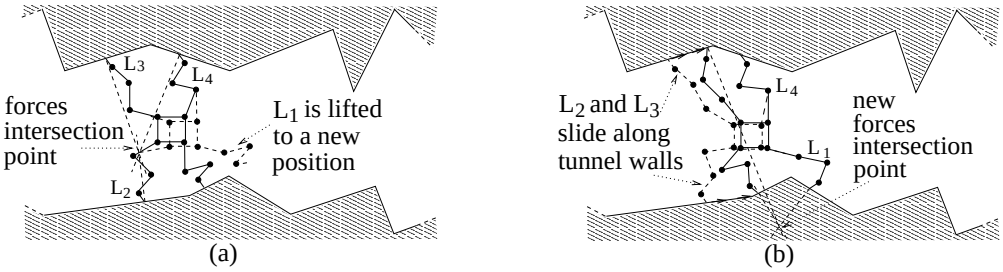

Figure 14: The two motion phases of a four-legged spider. (a) Limb lifting of L_1. (b) Limb repositioning in preparation for the lifting of L_4.

yields a simple motion paradigm, whereby the spider merely has to select non-redundant 4-contact equilibrium postures in order to ensure its immobilization.

Next we describe a motion paradigm for the four-legged spider robot depicted in Figure 1(b). This robot must use second-order effects in order to immobilize itself, and its motion consists of the following two phases. In the first phase, called *limb lifting*, the spider braces against the environment with three limbs while moving its fourth limb to a new foothold position. During this motion the central base and the three limbs contacting the environment move in a way which keeps the contacting footpads stationary with respect to the environment. At the end of a limb-lifting phase all four limbs contact the environment. However, before the spider can lift a new limb, it must ensure that the remaining three limbs form an equilibrium posture. For clarity, let the limbs be denoted L_1, L_2, L_3, L_4. Suppose that the spider initially lifts the limb L_1, while the limbs L_2, L_3, L_4 maintain a 3-legged equilibrium posture (Figure 14(a)). To be able to lift a new limb, say L_4, the spider must first ensure that the force-lines of the limbs L_1, L_2, L_3 intersect at a common point. However, the limbs L_2 and L_3 are common to both limb-triplets, and the force-lines of L_2 and L_3 intersect at a unique point. Hence we must first move the contact points of the limbs L_2 and L_3 with the tunnel walls before the limb L_4 can be lifted.

In the second phase, called *limb repositioning*, the spider slides two limbs along the tunnel walls, while the other two limbs maintain a fixed contact with the environment. For example, in Figure 14(b) the spider slides the limbs L_2 and L_3 along the tunnel walls, while the limbs L_1 and L_4 maintain a fixed contact with the environment. During this sliding, the intersection point of the force-lines of the limbs L_2 and L_3 moves forward, until it reaches the stationary force-line of L_1. Now the limbs L_1, L_2, L_3 form a 3-legged equilibrium posture, and the spider can lift the limb L_4. Note that in both modes of locomotion the spider is continuously immobile with respect to the tunnel walls. During limb repositioning the spider is immobilized by first-order effects, while during limb lifting the spider is immobilized by a combination of first and second-order effects.

C Details of the Stability Proof

In this appendix we first sketch the proof of Lemma 3.1, then give formulas for the partial derivatives of δ_i.

Lemma 3.1 *Let p^* be a spider configuration at which m limbs ($3 \leqslant m \leqslant k$) press against the environment in an equilibrium posture. Let δ_i^* ($i = 1, ..., m$) be the footpad penetrations*

corresponding to p^*. Then there exist intermediate penetration values, $0 < \hat{\delta}_i < \delta_i^*$ $(i = 1, ..., m)$, at which the closed-loop system (8) is at an equilibrium.

Proof sketch: To begin with, the limbs that do not contact the environment are influenced only by their joint actuators. These limbs form an equilibrium at $p_i = p_i^*$ for $i = m+1, ..., k$. Next consider the limbs that contact the environment. Let δ_i^* $(i = 1, ..., m)$ denote the amount of penetration corresponding to the target configuration p^*. By construction, at p^* the tunnel's reaction forces generate zero net wrench on the central-base:

$$\left.\frac{\partial}{\partial p_0}\right|_{p=p^*} \Pi(p_0, \bar{p}) = \sum_{i=1}^{m} \kappa \delta_i^* \begin{pmatrix} N_i \\ N_i \times R r_i \end{pmatrix} = 0_{3\times 1}, \tag{17}$$

where we have assumed a linear compliance relationship with a uniform material stiffness κ. In this formula N_i is the i^{th} contact normal; r_i is the endpoint of the overlap segment on the boundary of the i^{th} footpad, expressed in the central-base frame; and R is the central-base orientation matrix. The equilibrium posture (17) induces a family of equilibrium postures, obtained by pressing the footpads along the contact normals N_i starting from zero penetration. Assuming that R remains constant, the normals N_i and the vectors $N_i \times R r_i$ do not vary along normal penetration of the footpads. Hence $\frac{\partial}{\partial p_0}\Pi(p_0, \bar{p}) = 0$ along any normal penetration with $\delta_i = s\delta_i^*$ for $i = 1, ..., m$, where $s \in [0, 1]$.

Let us assume that during the normal penetration, the spider's central-base maintains a fixed configuration p_0^0. This assumption is kinematically feasible if each of the spider's limbs has at least three degrees of freedom. Let x_i denote the representation of the point r_i in a world frame. Then for a fixed central-based location, x_i varies as a function of the i^{th} limb configuration p_i. Assuming a linear compliance relationship, the i^{th} limb joint torques due to the i^{th} reaction force are: $-\frac{\partial}{\partial p_i}\Pi(p_0^0, \bar{p}) = \kappa\delta_i [Dx_i(p_i)]^T N_i$. Let the closed-loop spider system obey the PD rule (6), such that $P = diag(P_1, ..., P_k)$ where each P_i is an $n \times n$ positive definite matrix. Then the second part of the equilibrium condition (9) can be written as:

$$P_i(p_i - p_i^*) = \kappa\delta_i [Dx_i(p_i)]^T N_i \quad i = 1, ..., m.$$

Multiplying both sides by P_i^{-1} and then by $Dx_i(p_i)$ gives:

$$Dx_i(p_i)(p_i - p_i^*) = \kappa\delta_i [Dx_i(p_i)] P_i^{-1} [Dx_i(p_i)]^T N_i.$$

However, we may assume that p_i^* is close to p_i, and in this case $[Dx_i(p_i)](p_i - p_i^*) \cong x_i - x_i^*$ where $x_i^* = x_i(p^*)$. Thus we have the approximate relation:

$$x_i - x_i^0 = x_i^* - x_i^0 + \kappa\delta_i [Dx_i(p_i)] P_i^{-1} [Dx_i(p_i)]^T N_i, \tag{18}$$

where x_i^0 is the original contact point corresponding to zero penetration. During a normal penetration process, the point x_i moves along the negated normal N_i from x_i^0 toward x_i^*. Thus we have that $\delta_i = (x_i - x_i^0) \cdot (-N_i)$ and $\delta_i^* = (x_i^* - x_i^0) \cdot (-N_i)$. Taking the scalar product of both sides of (18) with $-N_i$ gives the following expression in the unknown δ_i:

$$\delta_i = \delta_i^* - \kappa\delta_i N_i^T [Dx_i(p_i)] P_i^{-1} [Dx_i(p_i)]^T N_i. \tag{19}$$

The term $N_i^T [Dx_i(p_i)] P_i^{-1} [Dx_i(p_i)]^T N_i$ is non-negative and depends on δ_i in a complex way. However, we can determine the essential properties of the solution δ_i for (19) as follows.

First, (19) can be written as $\delta_i(1+\kappa N_i^T[Dx_i(p_i)]P_i^{-1}[Dx_i(p_i)]^T N_i) = \delta_i^*$. The left side of the latter equation varies in $[0,\infty)$ as δ_i varies in $[0,\infty)$. Hence there exist at least one solution for δ_i in (19). Second, (19) can also be written as

$$\delta_i = \frac{1}{1+\kappa N_i^T[Dx_i(p_i)]P_i^{-1}[Dx_i(p_i)]^T N_i}\delta_i^*.$$

Hence all solutions for δ_i in (19), denoted $\hat{\delta}_i$, satisfy $0 < \hat{\delta}_i < \delta_i^*$ for $i = 1,...,m$. The penetration values $\hat{\delta}_i$ are the ones that satisfy the equilibrium condition (9). □

Formulas for the partial derivatives of δ_i. The lower bounds for the controller's stiffness parameters are expressed in terms of the partial derivatives of δ_i. We give formulas for these derivatives assuming semi-circular footpads penetrating piecewise-linear tunnel walls. This case has been discussed in Appendix A, where we derived a formula for δ_i as a function of a rigid-body configuration $q \in I\!R^3$. However, now δ_i is a function of the entire spider configuration $p \in I\!R^{nk+3}$. Recall that z_i is the position of the i^{th} footpad center-of-curvature, expressed in the central-base frame. Then z_i is a function of the i^{th} limb joints p_i. Recall, too, that the central-base configuration, p_0, is parametrized as $p_0 = (d,\theta) \in I\!R^3$. Then the expression for δ_i derived in Appendix A now takes the form: $\delta_i(p) = c_i - (R(\theta)z_i(p_i)+d)\cdot N_i$, where c_i is a constant specified above. The gradient vector $\nabla\delta_i(p)$ contains the partial derivatives $\frac{\partial}{\partial p_0}\delta_i(p)$ and $\frac{\partial}{\partial p_i}\delta_i(p)$. These derivatives are given by

$$\frac{\partial}{\partial p_0}\delta_i(p) = -\begin{pmatrix} N_i \\ Rz_i \times N_i \end{pmatrix} \quad \text{and} \quad \frac{\partial}{\partial p_i}\delta_i(p) = -[Dz_i(p_i)]^T R^T N_i,$$

where $u \times v$ denotes the scalar $\det[uv]$. Next, the formula for $D^2\delta_i(p)$ contains the partial derivatives $\frac{\partial^2}{\partial^2 p_i}\delta_i(p)$ and $\frac{\partial}{\partial p_i}\frac{\partial}{\partial p_0}\delta_i(p)$. Denoting the joints of the i^{th} limb by $\theta_{i1},...,\theta_{in}$, these derivatives are given by

$$\frac{\partial^2}{\partial^2 p_0}\delta_i(p) = \begin{bmatrix} 0_{2\times 2} & 0 \\ 0 & Rz_i \cdot N_i \end{bmatrix}_{3\times 3} \qquad \frac{\partial}{\partial p_i}\frac{\partial}{\partial p_0}\delta_i(p) = \begin{bmatrix} 0_{2\times n} \\ -N_i^T[DR(\theta)]Dz_i(p_i) \end{bmatrix}_{3\times n}$$

and

$$\frac{\partial^2}{\partial^2 p_i}\delta_i(p) = \begin{bmatrix} \left(\frac{\partial^2 z_i}{\partial^2\theta_{i1}}\right)^T R^T N_i & \cdots & \left(\frac{\partial^2 z_i}{\partial\theta_{in}\partial\theta_{i1}}\right)^T R^T N_i \\ \vdots & & \vdots \\ \left(\frac{\partial^2 z_i}{\partial\theta_{i1}\partial\theta_{in}}\right)^T R^T N_i & \cdots & \left(\frac{\partial^2 z_i}{\partial^2\theta_{in}}\right)^T R^T N_i \end{bmatrix}_{n\times n}.$$

References

[1] J.-D. Boissonnat, O. Devillers, L. Donati, and F. P. Preparata. Motion planning for spider robots. In *IEEE Int. Conf. on Robotics and Automation*, pages 2321–2326, 1992.

[2] G.S. Chirikjian and J.W. Burdick. Design and experiments with a 30 degree-of-freedom hyper-redundant robot. In *IEEE Int. Conf. on Robotics and Automation*, pages 3:113–117, 1993.

[3] S. Dubowsky, C. Sunada, and C. Marvoidis. Coordinated motion and force control of multi-limbed robotic systems. *Autonomous Robots*, 6:7–20, 1999.

[4] D.G. Flom. Dynamic mechanical losses in rolling contacts. In J.B. Bidwell, editor, *Rolling Contact Phenomena*, pages 97–112. Elsevier, 1962.

[5] H. Hertz. On the contact of elastic solids. In *Miscellaneous Papers by H. Hertz (1882).* Macmillan, London, 1896.

[6] S. Hirose and O. Kunieda. Generalized standard foot trajectory for a quadruped walking vehicle. *The Int. J. of Robotics Research*, 10(1):2–13, 1991.

[7] S. Hirose and A. Morishima. Design and control of a mobile robot with an articulated body. *The Int. J. of Robotics Research*, 9(2):99–114, 1990.

[8] N. Hogan. Impedance control: An approach to manipulation—part i, part ii, part iii. *ASME J. Dynamic Syst., Measure., Control*, 107:1–24, 1985.

[9] W. S. Howard and V. Kumar. On the stability of grasped objects. *IEEE Transactions on Robotics and Automation*, 12(6):904–917, Dec. 1996.

[10] K. L. Johnson. *Contact Mechanics.* Cambridge University Press, 1985.

[11] D. E. Koditschek. The application of total energy as a lyapunov function for mechanical control systems. *In J. Marsden, Krishnaprasad, and J. Simo, editors, Control Theory and Multibody Systems, AMS Series in Contemporary Mathematics*, 97:131–158, 1989.

[12] Q. Lin, J. W. Burdick, and E. Rimon. Computation and analysis of compliance in grasping and fixturing. In *IEEE Int. Conf. on Robotics and Automation*, pages 93–99, 1997.

[13] A. Madhani and S. Dubowsky. Motion planning of mobile multi-limb robotic systems subject to force and friction constraints. In *IEEE Int. Conf. on Robotics and Automation*, pages 233–239, 1992.

[14] D. W. Marhefka and D. E. Orin. Gait planning for energy efficiency in walking machines. In *IEEE Int. Conf. on Robotics and Automation*, pages 474–480, 1997.

[15] T. McGeer. Powered flights, child's play, silly wheels and walking machines. In *IEEE Int. Conf. on Robotics and Automation*, pages 1592–1597, 1989.

[16] W. Neubauer. Spider-like robot that climbs vertically in ducts or pipes. In *IEEE/RSJ/GI International Conference on Intelligent Robots and Systems*, pages 2:1178–1185, 1994.

[17] V.-D. Nguyen. Constructing stable grasps. *The Int. Journal of Robotics Research*, 8(1):27–37, 1988.

[18] F. Pfeiffer, F. Chernousko, N. Bolotnik, T. Robmann, and G. Kostin. Tube-crawling robot: Modeling and optimization. *To appear in: IEEE Trans. on Robotics and Automation*, 2000.

[19] J. Ponce. On planning immobilizing fixtures for 3d polyhedral parts. In *IEEE Int. Conf. on Robotics and Automation*, pages 509–514, 1996.

[20] E. Rimon and J. W. Burdick. Mobility of bodies in contact—i: A 2^{nd} order mobility index for multiple-finger grasps. *IEEE Trans. on Robotics and Automation*, 14(5):696–708, 1998.

[21] E. Rimon and J. W. Burdick. Mobility of bodies in contact—ii: How forces are generated by curvature effects. *IEEE Trans. on Robotics and Automation*, 14(5):709–717, 1998.

[22] E. Rimon, S. Shoval, and A. Shapiro. Design of a spider robot for motion with quasistatic force constraints. *Autonomous Robots (to appear)*, http://www.technion.ac.il/~robots.

[23] T. Roassmann and F. Pfeiffer. Control and design of a pipe crawling robot. In *13th World Congress of Automatic Control*, San Francisco, USA, 1996.

[24] J. M. Selig. *Geometrical Methods in Robotics*. Springer Verlag, New York, 1996.

[25] Y. Shan and Y. Koren. Design and motion planning of a mechanical snake. *IEEE Trans. on Systems Man and Cybernetics*, 23(4):1091–1100, 1993.

[26] T. J. Stone, D. S. Cook, and B. L. Luk. Robug iii - the design of an eight legged teleoperated walking and climbing robot for disordered hazardous environments. *Mechanical Incorporated Engineer*, 7(2):37–41, 1995.

[27] Sir W. Thompson and P. G. Tait. *Treatise on Natural Philosophy*. University of Cambridge Press, 1886, Cambridge.

[28] S. P. Timoshenko and J. N. Goodier. *Theory of elasticity*. McGraw-Hill, New York, 3rd edition, 1969.

[29] J. C. Trinkle. On the stability and instantaneous velocity of grasped frictionless objects. *IEEE Transactions on Robotics and Automation*, 8(5):560–572, Oct 1992.

[30] K. van der Doel and D. K. Pai. Performance measures for locomotion robots. *J. of Robotic Systems*, 14(2):135–147, 1997.